

ENHANCING THE CROSS-SIZE GENERALIZATION FOR SOLVING VEHICLE ROUTING PROBLEMS VIA CONTINUAL LEARNING

Jingwen Li¹, Zhiguang Cao², Yaxin Wu^{3,†}, Tang Liu¹

¹Sichuan Normal University ²Singapore Management University ³Eindhoven University of Technology

{lijingwen, liutang}@sicnu.edu.cn

zhiguangcao@outlook.com

wyxacc@hotmail.com

†Corresponding author

ABSTRACT

Exploring machine learning techniques for addressing vehicle routing problems has attracted considerable research attention. To achieve decent and efficient solutions, existing deep models for vehicle routing problems are typically trained and evaluated using instances of a single size. This substantially limits their ability to generalize across different problem sizes and thus hampers their practical applicability. To address the issue, we propose a continual learning based framework that sequentially trains a deep model with instances of ascending problem sizes. Specifically, on the one hand, we design an inter-task regularization scheme to retain the knowledge acquired from smaller problem sizes in the model training on a larger size. On the other hand, we introduce an intra-task regularization scheme to consolidate the model by imitating the latest desirable behaviors during training on each size. Additionally, we exploit the experience replay to revisit instances of formerly trained sizes for mitigating the catastrophic forgetting. Experimental results show that our approach achieves predominantly superior performance across various problem sizes (either seen or unseen in the training), as compared to state-of-the-art deep models including the ones specialized for generalizability enhancement. Meanwhile, the ablation studies on the key designs manifest their synergistic effect in the proposed framework.

1 INTRODUCTION

Combinatorial optimization problems hold significant practical value to various application domains (Korte et al., 2011). Among these, vehicle routing problems (VRPs), exemplified by the traveling salesman problem (TSP) and the capacitated vehicle routing problem (CVRP), stand as quintessential representatives. VRPs aim to find the optimal route for vehicles serving a group of customers in various real-life scenarios, such as parcel pickup/delivery, passenger transportation, and home health care (Baker & Ayechew, 2003; Schneider et al., 2014). Despite the extensive efforts in computer science and operations research, traditional exact and heuristic algorithms still encounter challenges when solving VRPs due to their NP-hard nature (Lenstra & Kan, 1981). These algorithms often require massive tuning to determine the hand-crafted rules and related hyperparameters. To mitigate this issue, deep (reinforcement) learning based methods have been extensively studied and applied to solve VRPs in recent years (Bengio et al., 2021; Zhang et al., 2023a), which leverage neural networks to automatically learn (heuristic) policies from the experience of solving similar VRP instances. Bolstered by advanced neural networks and training approaches, some of these deep models have achieved competitive or even superior performance to the traditional algorithms (Li et al., 2021b; 2023; Kong et al., 2024; Sun et al., 2019).

Typically, existing deep models are often trained and evaluated on single-sized problem instances, where they are able to deliver decent and efficient solutions. However, the performance of learned policies diminishes when applied to sizes not encountered during the training phase. This limitation becomes more pronounced as the disparity between the sizes further increases. Such a cross-size

generalization issue considerably hinders the applications of deep models, especially given that real-world VRP instances consistently present a diverse range of problem sizes.

To address this issue, we propose a continual learning (CL) (Chen & Liu, 2018) based framework that sequentially trains a deep model on instances of ascending problem sizes. This approach enables the model to perform favorably across a range of problem sizes, covering both those seen and unseen during the training phase. Specifically, we preserve exemplary models derived from the previous training, and leverage the regularization scheme to retain their knowledge for facilitating the subsequent training. We design two distinct regularization terms in the loss function, i.e., the inter-task and the intra-task regularization terms. During the training on each size, the former aims to transfer the valuable insights from smaller-sized tasks to larger-sized ones, while the latter enables the imitation of the most recent exemplar models. Intuitively, both schemes expedite the training on a newly encountered size, with the aid of previously attained experience in problem solving. Additionally, we tailor an experience replay technique (Rolnick et al., 2019) to intermittently revisit the instances of previously trained smaller sizes for mitigating the catastrophic forgetting (French, 1999). Notably, the proposed continual learning only improves the training algorithm of existing deep models, without altering their original neural architectures. It has a great potential to be deployed with different models, without inducing extra inference time. Experimental results indicate that our approach significantly raises the cross-size generalization performance of deep models for both seen and unseen problem sizes. Furthermore, it generally outperforms the state-of-the-art methods that are specially designed for enhancing the generalizability of deep models, showing the effectiveness of our algorithmic designs.

Accordingly, our contributions are summarized as follows: (1) We propose a model-agnostic continual learning based framework to improve the cross-size generalization capabilities of deep models for VRPs. With a single training session, the proposed approach empowers deep models to deliver promising results for VRPs across a wide range of problem sizes, without incurring extra inference time. (2) To expedite the training on new sizes, we design the inter-task regularization scheme to facilitate the knowledge transfer from smaller to larger sizes. Alternatively, the intra-task regularization scheme consolidates the model by imitating the most recent exemplar models on the current size. On the other hand, we employ the experience replay to counteract the catastrophic forgetting, retaining the competence of deep model in handling smaller-size instances beyond its training on larger ones. (3) We evaluate our approach on TSP and CVRP across a wide range of sizes (seen or unseen during the training). Results on both synthetic and (real-world) benchmark datasets show that our approach bolsters the cross-size generalization, yielding predominantly superior performance to the state-of-the-art methods specialized for generalizability enhancement.

2 RELATED WORK

In this section, we review deep models for VRPs and representative works on enhancing cross-size generalization. Then, we brief on the generic continual learning in the machine learning community.

Deep models for VRPs. Recent learning based methods, i.e., deep models, have shown promise in solving VRPs by automatically discovering effective policies. Vinyals et al. (2015) tendered the Pointer network to learn constructing TSP solution supervisedly, which was further extended to reinforcement learning (Bello et al., 2017) and CVRP (Nazari et al., 2018). Similarly, the graph conventional network (GCN) was leveraged to estimate probabilities of each edge appearing in the optimal TSP solution (Joshi et al., 2019). With recent advances of the self-attention mechanism, the attention model (AM) (Kool et al., 2018) was tailored from Transformer (Vaswani et al., 2017) for solving VRPs and recognized as a landmark contribution in this field. The follow-up works diverged by (slightly) restructuring AM or targeting diverse VRP variants (Xin et al., 2020; Li et al., 2021a). The policy optimization with multiple optima (POMO) (Kwon et al., 2020) improved AM by exploiting symmetric rollouts and data augmentation technique, achieving state-of-the-art performance for VRPs. Despite the efficient inference, the above methods usually require heavy post-processing procedures to enhance solution quality, such as sampling (Li et al., 2021b), active search (Hottung et al., 2021). Especially, some works attempt to improve the generalization performance of deep models in handling distribution shift (Jiang et al., 2022; Bi et al., 2022; Hottung et al., 2021; Zhou et al., 2023). Instead, this paper aims to enhance the cross-size generalization towards a deep model capable of well solving different-sized VRPs.

Cross-size generalization. The above deep models are often trained to solve single-sized VRP instances for attaining favorable evaluation results on that problem size. However, their performance degenerates when the models are evaluated on sizes unseen during the training. To address this cross-size generalization issue, Lisicki et al. (2020) proposed a curriculum learning method to solve TSP instances spanning a range of problem sizes. Similarly, Zhang et al. (2023b) utilized the curriculum learning to train a deep model on different-sized TSP, with the knowledge distillation used for training on the largest TSP. Nevertheless, both methods are limited to TSP and lack the versatility in addressing broader VRP variants. Instead, Zhou et al. (2023) worked on improving generalization performance across sizes and distributions, by introducing a meta-learning approach to initialize deep models for rapid adaptation to target VRPs. However, its performance is contingent on the heavy base model and tricky meta-learning process, which could suffer from a high training cost in the absence of well pre-trained deep models.

In this paper, we first use continual learning to enhance cross-size. Note that our work is different from the ones attempting to solve large-scaled VRPs, which require extra inefficient training/post-processing for the target size (Qiu et al., 2022; Sun & Yang, 2023; Li et al., 2021c; Fu et al., 2021; Hou et al., 2022; Zong et al., 2022). Our overarching goal is developing a single model with favorable performance in a broad spectrum of problem sizes, in only a single training session.

Continual learning. Continual learning (CL) is advantageous in sequentially learning a stream of relevant tasks by absorbing and accumulating knowledge over them (Hadsell et al., 2020). However, CL is generally limited by catastrophic forgetting, where learning a new task usually results in a performance degradation on the old tasks. To address this issue, numerous efforts have been devoted in recent years to strike a desirable balance between learning plasticity and memory stability. These works can be broadly categorized into three groups, i.e., regularization-based approaches (Li & Hoiem, 2017) that regularize the current training with the knowledge acquired in the past training; replay-based approaches (Rebuffi et al., 2017) that revisit data distributions of previous tasks; and parameter isolation approaches (Mallya & Lazebnik, 2018) that freeze parameters associated with earlier tasks. Continual learning has widespread applications in visual classification (He & Zhu, 2021), semantic segmentation (Michieli & Zanuttigh, 2019), natural language processing (Han et al., 2021), to name a few. We direct interested readers to (De Lange et al., 2021; Parisi et al., 2019) for more details of CL. In this paper, we introduce the continual learning into VRP domain, and empirically testify its potential in training deep models that favorably solve different-sized VRPs.

3 PRELIMINARIES AND NOTATIONS

We first formally describe the vehicle routing problems (VRPs) with the objective of yielding high-quality solutions across a spectrum of problem sizes. Then, we present the commonly used encoder-decoder structured deep models for constructing solutions to VRPs in an autoregressive manner.

3.1 VRP STATEMENT

Following the literature (Kool et al., 2018; Wu et al., 2021), we focus on two representative routing problems, i.e., TSP and CVRP, respectively. We define a VRP instance over a graph $G = (V, E)$, where V signifies (customer) nodes and E signifies edges between every two different nodes. With N customer in different locations, TSP aims to find the shortest Hamiltonian cycle of $V = \{v_i\}_1^N$, which satisfies that each node in V is visited exactly once. With an auxiliary depot node v_0 , CVRP extends TSP by considering a fleet of identical vehicles, each of which traverses locations of customers for serving them. Specifically, each vehicle starts from the depot, serves a subset of customers and ultimately returns to the depot. The constraint on the route of a vehicle is that the total demand of customers in a route cannot exceed the vehicle capacity and each customer is visited exactly once.

Objective Function. The solution (i.e., tour) τ^N to a VRP instance can be described as a permutation of N nodes in V . The objective function is often defined as the tour length. For example, the objective function of TSP is $C(\tau^N) = \sum_{\{v_i, v_j\} \in \tau^N} D(v_i, v_j)$, where $D(v_i, v_j)$ means the Euclidean distance between the nodes v_i and v_j . In this paper, we focus on optimizing objective values of VRPs across multiple problem sizes. By referring various sizes to a series $\{N_1, N_2, \dots, N_K\}$, the cross-size objective function could be defined as the average value of the expected tour lengths over the K sizes, i.e., $L = \frac{1}{K} \sum_{i=1}^K \mathbb{E}[C(\tau^{N_i})]$, reflecting the overall performance of deep models.

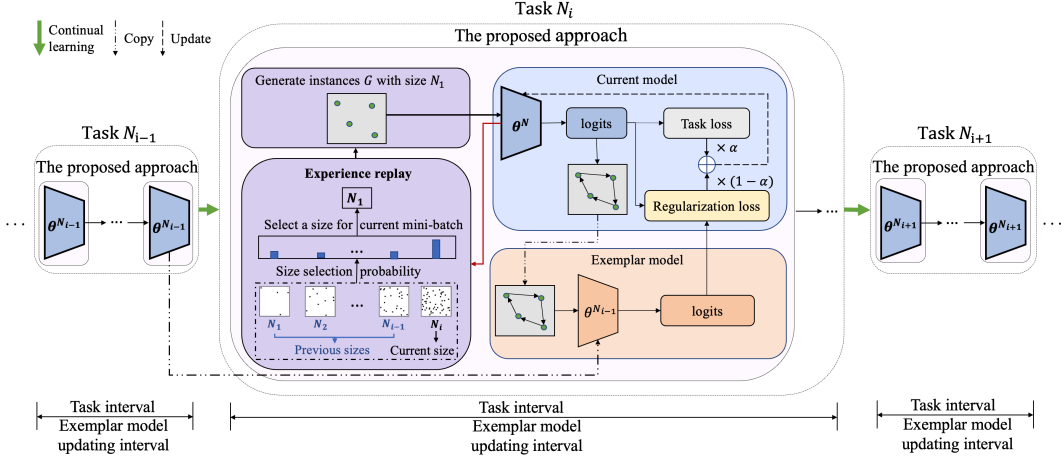


Figure 1: The illustration of the proposed framework with inter-task regularization. For each mini-batch training during current task interval, we employ 1) experience replay to sample a size from formerly trained sizes and current one, and generate instances with that sampled size; 2) inter-task regularization to foster the current model to emulate an exemplary model for knowledge retention.

3.2 AUTOREGRESSIVE DEEP MODELS FOR VRPs

Deep models often learn constructing solutions to TSP instances in an autoregressive manner. Specifically, they model the solution construction procedure of VRPs as a Markov Decision Process (MDP). Then the encoder-decoder structured policy network is adopted to sequentially construct solutions. More specific, the encoder projects problem-specific features into high-dimensional node embeddings for informative representation learning. Afterwards, the decoder sequentially constructs a solution τ^{N_i} for a TSP instance of problem size N_i , conditioned on the updated node embeddings and partial tour at each step. During solution construction, the decoder selects a node a_{t_c} at step t_c , with all constraints satisfied by masking the invalid nodes. A feasible solution is constructed until all customer nodes are selected, which is expressed by the factorization below,

$$p_\theta(\tau^{N_i} | G) = \prod_{t_c=1}^{T_c} p_\theta(a_{t_c} | a_{1:t_c-1}, G), \quad (1)$$

where p_θ and T_c signifies the policy network and the total number of decoding steps, respectively. In particular, $T_c = N_i$ for TSP, and $T_c \geq N_i$ for CVRP as the depot node can be visited multiple times.

4 METHODOLOGY

Continual learning has emerged as a powerful approach for handling sequential tasks, which enables deep models to progressively retain and accumulate knowledge from evolving data streams. As illustrated in Figure 1, we harness CL to enhance the cross-size generalization capability of an autoregressive deep model θ (e.g., POMO (Kwon et al., 2020) (see Appendix E for details)), by sequentially training it on VRP instances of ascending problem sizes $\{N_1, N_2, \dots, N_K\}$. To ensure general favorable performance across the size spectrum, each size (i.e., task) N_i ($i = 1, \dots, K$) is considered equally important and trained with the same task interval, which is defined as $E_p = E/K$ epochs where E denotes the total training epochs of CL. In each task interval, the model is trained on each size to optimize the task-specific objective. Meanwhile, our approach exploits experience replay strategy to revisit instances of previously trained smaller sizes, so as to mitigate the catastrophic forgetting. Moreover, the inter-task or intra-task regularization scheme foster the model in current interval to emulate an exemplary model derived from previous or current interval, so as to inherit the previous learned knowledge. In this sense, our CL approach facilitates a coherent continuum of learning across varying problem sizes, which is elaborated in the following sections.

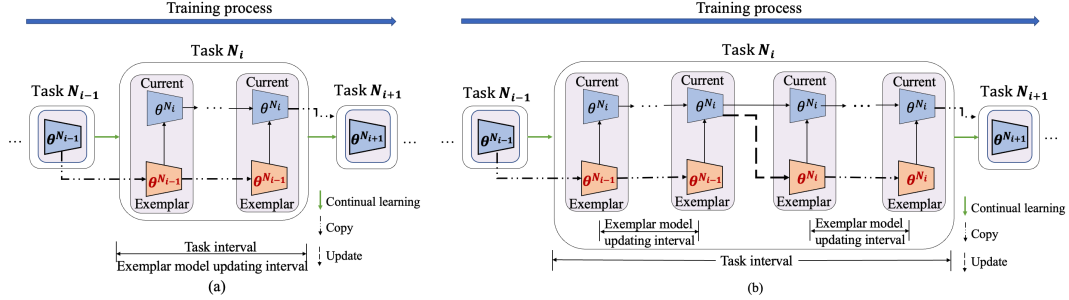


Figure 2: Regularization with two exemplar model updating strategies. (a) inter-task: exemplar model is updated after training on a whole task; (b) intra-task: exemplar model is updated multiple times during training on a task for concentrating more on newly encountered (larger) size.

4.1 EXPERIENCE REPLAY

Experience replay has shown promise to alleviate the catastrophic forgetting issue in continual learning, with the basic logic of reminding the model about the policy learned for previous tasks. A typical experience replay technique is to maintain a small memory buffer of training samples. These samples are collected from the past tasks and replayed during the training on subsequent tasks. Given that existing deep models for VRPs are generally trained with random instances (Kool et al., 2018; Kwon et al., 2020), we propose to randomly generate instances of smaller sizes on the fly. Such real-time memory buffer is able to reflect the instance patterns in previous tasks and raise the memory efficiency, when the deep model is trained on a newly encountered larger size.

During the training on the problem size N_i ($i > 1$), we harness a sampling strategy to either randomly select a size from the set of formerly trained sizes $N_{pre} = \{N_1, \dots, N_{i-1}\}$, or deterministically select the current size N_i . This strategy is devised to ensure that the deep model is primarily trained on the current task, i.e., the VRP with a larger size and higher complexity than the previous ones. Meanwhile, it ensures the competence of the deep model is retained for well solving previous tasks, i.e., the VRPs with smaller sizes but subjected to the catastrophic forgetting. To this end, we sample problem sizes in mini-batches during the training on size N_k , by assigning a higher probability to select N_i and a lower probability to uniformly select one from N_{pre} , such that,

$$N_k = \begin{cases} N_i, & \text{if } \epsilon < 0.5 \\ N_j \sim U(N_{pre}), & \text{otherwise} \end{cases} \quad (2)$$

where $\epsilon \in (0, 1)$ is a random number. Specially, only the size N_1 is involved in the first task.

4.2 REGULARIZATION SCHEMES

During the training process, we employ favorable models trained previously as the *exemplar* ones to infuse the *current* model with a wealth of knowledge in VRP solving, with the goal to guide the training on the newly encountered size. Specifically, we design two distinct terms in the loss function, i.e., inter-task regularization term and intra-task regularization term, respectively, with different update rule for the exemplar model. Note that only one regularization scheme can be used in our CL approach to keep a stable update of the exemplar model throughout the training.

Inter-task regularization scheme. As shown in Figure 2(a), the inter-task regularization scheme aims to retain knowledge derived from the past training on smaller sizes for achieving generalization across various sizes. Specifically, when training on size N_i , the current model θ^{N_i} is thoughtfully guided by the exemplar model $\theta^{N_{i-1}}$ meticulously trained on the preceding size N_{i-1} . In this fashion, the exemplar model is updated after training on each size, with the update interval equal to the task interval, i.e., $E_{inter} = E_p$. This strategy encourages the current model to imitate the solution construction policy learned by the exemplar model. Given a training instance G with size N_i and a tour $\tau_{\theta^{N_i}}$ constructed by θ^{N_i} , we leverage the exemplar model $\theta^{N_{i-1}}$ to engender the same tour, resulting in the probability distribution $p_{\theta^{N_{i-1}}}(\tau_{\theta^{N_i}} | G)$. The inter-task regularization loss $\mathcal{L}_{R_{inter}}$ is defined as the similarity between probability distributions derived by θ^{N_i} and $\theta^{N_{i-1}}$ over a mini-

Algorithm 1: Model training by continual learning

Input: An ascending sequence of problem sizes N_1, N_2, \dots, N_K with equal space n ; a pre-trained backbone model (e.g., POMO) parameterized by θ^{N_1} on size N_1 ;

- 1: **for** epoch $e = 1, 2, \dots, E$ **do**
- 2: Compute the size $N_i = N_1 + n * (e \% E_p)$ of current task;
- 3: **for** step $t = 1, 2, \dots, T$ **do**
- 4: Pick a size $N_k, k = 1, \dots, i$ according to Eq. (2);
- 5: Randomly generate a batch of training instances with size N_k ;
- 6: Let model θ (e.g., θ^{N_i} for inter-task regularization) sample tours τ_θ^b for each $\{G_b\}_{b=1}^B$;
- 7: Compute $\nabla \mathcal{L}_R$ using Eq. (3) for inter-task regularization or Eq. (4) for intra-task one;
- 8: Compute $\nabla \mathcal{L}_T$ using Eq. (5);
- 9: $\theta \leftarrow \theta + \eta \nabla \mathcal{L}$ where $\nabla \mathcal{L} \leftarrow \alpha \nabla \mathcal{L}_R + (1 - \alpha) \nabla \mathcal{L}_T$.
- 10: **end for**
- 11: **end for**

batch of instances $\{G_b\}_{b=1}^B$, which is calculated by the Kullback-Leibler divergence as below,

$$\mathcal{L}_{R_{inter}} = \frac{1}{B} \sum_{b=1}^B \sum_{a_j \in \tau_{\theta^{N_i}}^b} p_{\theta^{N_{i-1}}}(a_j|G_b) (\log p_{\theta^{N_{i-1}}}(a_j|G_b) - \log p_{\theta^{N_i}}(a_j|G_b)). \quad (3)$$

Particularly, for training on the first size, a pre-trained backbone model (such as POMO (Kwon et al., 2020)) on size N_1 could be used to serve as the exemplar model in Eq. (3).

Intra-task regularization scheme. As illustrated in Figure 2(b), the intra-task regularization scheme concentrates more on consolidating the recently learned knowledge, thereby updating the exemplar model more frequently than inter-task scheme. Specifically, during the training on size N_i in the task interval, we update the exemplar model M times with an even update interval $E_{intra} = E_p/M$. Given the current epoch e , the training of the model $\theta_e^{N_i}$ is guided by the most recent exemplar model $\theta_m^{N_i}$ ($m = 1, 2, \dots, M$). Accordingly, the intra-task regularization loss $\mathcal{L}_{R_{intra}}$ over a mini-batch of instances $\{G_b\}_{b=1}^B$ is formulated as follows,

$$\mathcal{L}_{R_{intra}} = \frac{1}{B} \sum_{b=1}^B \sum_{a_j \in \tau_{\theta_e^{N_i}}^b} p_{\theta_m^{N_i}}(a_j|G_b) (\log p_{\theta_m^{N_i}}(a_j|G_b) - \log p_{\theta_e^{N_i}}(a_j|G_b)). \quad (4)$$

In contrast to inter-task regularization scheme using exemplar model from previous size, intra-task scheme adopts the one that has already been exposed to the intricacies of a new size, which could assimilate more generalized and resilient knowledge to boost the training efficiency and is preferred for generalizing to unseen larger sizes. However, the deep model cannot be sufficiently trained on a new size in the initial stage of a task interval. Thus we employ the finally well-established model $\theta_M^{N_{i-1}}$ on the last size as the exemplar, during the first E_{intra} epochs in the current task interval.

Finally, the deep model is trained with the objective of minimizing a weighted combination of the regularization term \mathcal{L}_R (i.e., $\mathcal{L}_{R_{inter}}$ for inter-task regularization and $\mathcal{L}_{R_{intra}}$ for intra-task regularization) and the original task loss \mathcal{L}_T , i.e., $\mathcal{L} = \alpha \mathcal{L}_R + (1 - \alpha) \mathcal{L}_T$, where $\alpha \in [0, 1]$. Taking inter-task regularization term as an example, the task loss is formulated as below,

$$\mathcal{L}_T = \mathbb{E}_{G \sim N_k, \tau^{N_k} \sim p_{\theta^{N_i}}(\tau^{N_k}|G)} [C(\tau^{N_k}|G)], \quad (5)$$

where the training instances are sampled with the selected size N_k via the experience replay strategy, and the tour τ^{N_k} is engendered via the current network θ^{N_i} according to Eq. (1). The task loss is used to update the deep model by REINFORCE (Williams, 1992), which is a commonly applied reinforcement learning algorithm in VRP literature (Kool et al., 2018; Kwon et al., 2020).

4.3 TRAINING ALGORITHM

We outline the training procedure of the proposed CL approach in Algorithm 1, where the model is sequentially trained using instances with ascending problem sizes N_1, \dots, N_K . Particularly, starting

with the training on size N_2 , the experience replay strategy plays the role to retain the competence in tackling smaller-size instances when addressing a new larger one. Moreover, the regularization scheme, i.e., either inter-task or intra-task, is smoothly incorporated during the whole training process, transferring previous valuable knowledge to facilitate the subsequent training. In this sense, the proposed approach is expected to endow the deep models with strong cross-size generalization ability so that they could perform favorably across a wide range of sizes.

5 EXPERIMENTS

To demonstrate the generality and effectiveness of the proposed framework, we apply it to two well-known and strong deep models, i.e., POMO (Kwon et al., 2020) and ELG (Gao et al., 2023), referred to as Ours-POMO and Ours-ELG, respectively. We conduct comprehensive experiments on two representative routing problems, i.e., TSP and CVRP (Kool et al., 2018; Wu et al., 2021), respectively.

Training setups. We adhere to most of the setups in POMO and ELG. For our approach, we set the ascending problem sizes $\{N_1, N_2, \dots, N_K\}$ to $\{60, 70, \dots, 150\}$ with $K = 10$. Note that these sizes could be flexibly adjusted to other incremental values. Regarding Ours-POMO, we set the training epochs to $E = 2000$, with instances of each size trained for $E_p = 200$ epochs, ensuring robust performance across the wide range of problem sizes. The update interval of the exemplar model is set to $E_{\text{inter}} = 200$ epochs for the inter-task regularization and $E_{\text{intra}} = 25$ epochs for the intra-task regularization. Regarding Ours-ELG, we follow the original design of ELG and set the training epochs to $E = 500$. Accordingly, the update interval of the exemplar model is set to $E_{\text{inter}} = 50$ epochs for the inter-task regularization and $E_{\text{intra}} = 10$ epochs for the intra-task regularization. Both Ours-POMO and Ours-ELG use a batch size of 64 (32 when the sizes exceed 100) for both TSP and CVRP.

Inference setups. Complying with the established convention (Kool et al., 2018), we randomly generate instances following the uniform distribution for both seen and unseen problem sizes during the training phase. Pertaining to the former, we select the three most representative sizes from the set of K training sizes aforementioned, encompassing the minimum size of 60 (with 10,000 instances), the median size of 100 (with 10,000 instances), and the maximum size of 150 (with 1,000 instances). Pertaining to the latter, we consider three larger unseen sizes, i.e., 200, 300 and 500 (with 128 instances for each), to further assess the generalizability. We conduct all experiments including the training and evaluation on a Linux server equipped with TITAN XP GPUs (with 12 GB memory) and Intel Xeon E5-2660 CPUs at 2.0 GHz. Our dataset and code in Pytorch will be made available.

5.1 COMPARISON ANALYSIS

We first verify the effectiveness of our approach on seen sizes during training for both TSP and CVRP, and the results are displayed in Table 1. Specifically, we compare our approach with 1) highly specialized VRP solvers: Concorde (Applegate et al., 2020) and LKH3 (Helsgaun, 2017) for TSP, the hybrid genetic search (HGS) (Vidal, 2022) and LKH3 for CVRP; 2) POMO-based methods, including the original POMO (Kwon et al., 2020), AMDKD-POMO (Bi et al., 2022) and Omni-POMO (Zhou et al., 2023); 3) recent learning-oriented routing solver ELG (specialized for enhancing generalization on complex node distributions and large problem sizes) (Gao et al., 2023) for both TSP and CVRP. For POMO and ELG, we retrain the model on each problem size with equal epochs as our approach for a fair comparison, e.g., *POMO-60* signifying the model trained on size 60, where POMO-random refers to the model trained on instances of random sizes within our training size range. AMDKD-POMO improved the cross-distribution generalization of POMO via knowledge distillation, where we retrain it following our training setups by tailoring teacher models to align with our exemplar sizes. Besides, we also show the results of its open-sourced pretrained models on the largest available sizes, i.e., AMDKD-POMO*. Furthermore, Omni-POMO is a recent meta-learning framework to improve generalization across size and distribution of POMO, where we report their results by directly using their open-sourced pretrained models. Regarding our approach, two distinct variations with inter-task and intra-task regularization schemes are denoted as *Ours-inter* and *Ours-intra*, respectively. Every method is assessed using data augmentation of POMO.

Table 1: Comparison results on TSP and CVRP (seen scales).

Method	Test on N=60			Test on N=100			Test on N=150			Average of Total costs	
	Obj.	Gap	Time	Obj.	Gap	Time	Obj.	Gap	Time		
Concorde	6.1729	-	(7m)	7.7646	-	(1.7h)	9.3462	-	(22m)	7.7612	
LKH3	6.1729	0.00%	(14m)	7.7646	0.00%	(9.8h)	9.3462	0.00%	(2.1h)	7.7612	
AMDKD-POMO*	6.1828	0.16%	36s	7.7930	0.37%	2m	9.4539	1.15%	33s	7.8092	
POMO-60	6.1746	0.03%	~	7.8050	0.52%	~	9.5909	2.62%	~	7.8568	
POMO-100	6.1768	0.06%	~	7.7753	0.14%	~	9.3987	0.56%	~	7.7836	
POMO-150	6.1928	0.32%	~	7.7875	0.30%	~	9.3812	0.36%	~	7.7868	
POMO-random	6.1778	0.08%	~	7.7823	0.23%	~	9.3937	0.51%	~	7.7846	
TSP	AMDKD-POMO	6.1820	0.15%	~	7.7916	0.35%	~	9.4473	1.08%	~	7.8070
	Omni-POMO [‡]	6.2351	1.01%	34s	7.8650	1.29%	2.5m	9.4958	1.60%	37s	7.8653
	Ours-POMO-inter	6.1763	0.06%	36s	7.7802	0.20%	2m	9.3912	0.48%	33s	7.7826
	Ours-POMO-intra	6.1767	0.06%	~	7.7807	0.21%	~	9.3891	0.46%	~	7.7822
	ELG-60	6.1772	0.07%	37s	7.8098	0.58%	1.3m	9.5593	2.28%	15s	7.8388
	ELG-100	6.1807	0.13%	~	7.7822	0.23%	~	9.4131	0.72%	~	7.7920
	ELG-150	6.1864	0.22%	~	7.7888	0.31%	~	9.4036	0.61%	~	7.7929
	ELG-random	6.1816	0.14%	~	7.7876	0.30%	~	9.4120	0.70%	~	7.7937
	Ours-ELG-inter	6.1789	0.10%	~	7.7867	0.29%	~	9.4078	0.66%	~	7.7911
	Ours-ELG-intra	6.1796	0.11%	~	7.7871	0.29%	~	9.4053	0.63%	~	7.7907
CVRP	HGS	11.9471	-	(15.3h)	15.5642	-	(25.6h)	19.0554	-	(6.2h)	15.5222
	LKH3	11.9694	0.19%	(3.5d)	15.6473	0.53%	(6.5d)	19.2208	0.87%	(13h)	15.6125
	AMDKD-POMO*	12.3561	3.42%	56s	15.8854	2.06%	3m	19.8395	4.12%	33s	16.0270
	POMO-60	12.0656	0.99%	~	16.0914	3.39%	~	20.2573	6.31%	~	16.1381
	POMO-100	12.2531	2.56%	~	15.7544	1.22%	~	19.6856	3.31%	~	15.8977
	POMO-150	12.4322	4.06%	~	15.8924	2.11%	~	19.3683	1.64%	~	15.8976
	POMO-random	12.2758	2.75%	~	15.7942	1.48%	~	19.6121	2.92%	~	15.8940
	AMDKD-POMO	12.1487	1.69%	~	15.8119	1.72%	~	19.5280	2.48%	~	15.8362
	Omni-POMO [‡]	12.2996	2.95%	45s	15.9878	2.72%	2.5m	19.5975	2.85%	45s	15.9616
	Ours-POMO-inter	12.0672	1.00%	56s	15.7903	1.45%	3m	19.4226	1.93%	33s	15.7600
	Ours-POMO-intra	12.0680	1.01%	~	15.7867	1.43%	~	19.4040	1.83%	~	15.7529
CVRP	ELG-60	12.0975	1.26%	56s	15.9834	2.69%	3.2m	19.8061	3.94%	52s	15.9557
	ELG-100	12.1397	1.61%	~	15.8382	1.76%	~	19.5446	2.57%	~	15.8408
	ELG-150	12.1920	2.05%	~	15.8862	2.07%	~	19.5197	2.44%	~	15.8660
	ELG-random	12.1612	1.79%	~	15.8717	1.98%	~	19.5405	2.55%	~	15.8578
CVRP	Ours-ELG-inter	12.1073	1.34%	~	15.8692	1.96%	~	19.5336	2.51%	~	15.8367
	Ours-ELG-intra	12.1110	1.37%	~	15.8617	1.91%	~	19.5208	2.44%	~	15.8312

Bold and *italics* refer to the best and the second-best performance, respectively, among all deep models.

~ The inference time of a method is equal to that of the preceding method in the row above, since those deep models except for Omni-POMO utilize the original POMO architecture and result in the same inference efficiency.

[‡] The training size range of Omni-POMO is [50, 200], which is broader than our [60, 150].

The total inference time is reported for all methods, i.e., GPU time for deep models and CPU time for traditional solvers.

From Table 1, we observe that our approach with intra-task regularization slightly outperforms the inter-task regularization variant on smaller problem sizes (e.g., 60 and 100 for TSP), but the other way round on larger sizes (e.g., 150 for TSP) for both Ours-POMO and Ours-ELG on TSP and CVRP. This is reasonable since intra-task regularization concentrate more on efficiently learning the latest larger sizes. Additionally, when compared to the original POMO and ELG models trained on a specific size, both Ours-POMO and Ours-ELG (incorporating either inter-task or intra-task regularization) exhibit competitive performance on those specific sizes for both TSP and CVRP. However, they significantly outperform the original POMO and ELG models in terms of average objective values across multiple problem sizes (see the final column). Regarding POMO-based methods, while specially designed to enhance the cross-distribution generalization of POMO, AMDKD-POMO* still suffers from the cross-size generalization issue. Furthermore, both Ours-POMO-inter and Ours-POMO-intra outperform POMO-random, AMDKD-POMO and Omni-POMO across all sizes for both TSP and CVRP with comparable inference time, even if Omni-POMO utilizes training instances with larger upper sizes (i.e., 200). Regarding ELG-based methods, while ELG models trained on specific sizes deliver slightly inferior performance to their POMO counterparts (e.g., POMO-60 vs. ELG-60), they demonstrate superior generalization performance on larger sizes (e.g., 150). This outcome is reasonable, as ELG employs an early stopping mechanism during POMO training to mitigate over-fitting, enhancing generalization at the potential expense of peak performance on those specific training sizes. Both Ours-ELG-inter and Ours-ELG-intra surpass ELG-random across all sizes for both TSP and CVRP, achieving better overall generalization (refer to the final column).

Table 2: Generalization results on TSP and CVRP (unseen scales).

Method	Test on N=200			Test on N=300			Test on N=500			Average of Total costs	
	Obj.	Gap	Time	Obj.	Gap	Time	Obj.	Gap	Time		
Concorde	10.6683	-	(8m)	12.9534	-	(11m)	16.5219	-	(17m)	13.3812	
LKH3	10.6683	0.00%	(25m)	12.9534	0.00%	(47m)	16.5219	0.00%	(1.2h)	13.3812	
AMDKD-POMO*	10.9651	2.78%	10s	13.9793	7.92%	33s	19.4197	17.54%	2.5m	14.7880	
POMO-60	11.3360	6.27%	~	14.8162	14.38%	~	20.5835	24.58%	~	15.5786	
POMO-100	10.8464	1.67%	~	13.8730	7.10%	~	20.1985	22.25%	~	14.9726	
POMO-150	10.7752	1.00%	~	13.2922	2.62%	~	18.0793	9.43%	~	14.0489	
POMO-random	10.8397	1.61%	~	13.8212	6.70%	~	19.0881	15.53%	~	14.5830	
TSP	AMDKD-POMO	10.9054	2.22%	~	13.4472	3.81%	~	18.4477	11.66%	~	14.2668
	Omni-POMO [‡]	10.8923	2.10%	11s	13.4044	3.48%	33s	17.8146	7.82%	2.6m	14.0371
	Ours-POMO-inter	10.7696	0.95%	10s	13.2723	2.46%	33s	17.8332	7.94%	2.5m	13.9584
	Ours-POMO-intra	10.7531	0.80%	~	13.2172	2.04%	~	17.7517	7.44%	~	13.9073
	ELG-60	11.0613	3.68%	4s	13.8150	6.65%	7s	18.2116	10.23%	15s	14.3626
	ELG-100	10.8280	1.50%	~	13.4278	3.67%	~	17.7035	7.15%	~	13.9864
	ELG-150	10.7821	1.07%	~	13.2802	2.52%	~	17.4444	5.58%	~	13.8356
	ELG-random	10.8131	1.36%	~	13.3886	3.36%	~	17.6597	6.89%	~	13.9538
	Ours-ELG-inter	10.7808	1.06%	~	13.2643	2.40%	~	17.3802	5.20%	~	13.8084
	Ours-ELG-intra	10.7770	1.02%	~	13.2360	2.18%	~	17.3045	4.74%	~	13.7725
	HGS	21.9737	-	(1.1h)	25.8417	-	(1.6h)	31.0308	-	(2.5h)	26.6514
	LKH3	22.2146	1.10%	(2.4h)	26.2184	1.46%	(3.2h)	31.5213	1.58%	(5.3h)	26.6514
	AMDKD-POMO*	23.8507	8.54%	12s	30.7218	17.18%	38s	48.1260	52.68%	3m	34.2328
	POMO-60	24.0638	9.51%	~	29.6416	14.71%	~	38.8480	25.19%	~	30.8511
	POMO-100	23.2783	5.94%	~	28.9372	11.98%	~	37.9132	22.18%	~	30.0429
	POMO-150	22.4706	2.26%	~	26.8810	4.02%	~	33.7746	8.84%	~	27.7087
	POMO-random	23.2016	5.59%	~	28.1393	8.89%	~	35.6822	14.99%	~	29.0077
	AMDKD-POMO	22.7842	3.69%	~	27.4462	4.68%	~	34.0650	9.78%	~	28.0985
	Omni-POMO [‡]	22.6562	3.11%	13s	26.8707	3.98%	38s	33.1435	6.81%	4m	27.5568
	Ours-POMO-inter	22.4981	2.39%	12s	26.7699	3.59%	38s	33.2138	7.04%	3m	27.4939
	Ours-POMO-intra	22.4523	2.18%	~	26.6468	3.12%	~	33.0600	6.54%	~	27.3864
	ELG-60	23.2704	5.90%	14s	27.9584	8.19%	39s	35.4367	14.20%	2.4m	28.8885
	ELG-100	22.7460	3.52%	~	27.1748	5.16%	~	33.4630	7.84%	~	27.7946
	ELG-150	22.6514	3.08%	~	26.9530	4.30%	~	33.0651	6.56%	~	27.5565
	ELG-random	22.7191	3.39%	~	27.1218	4.95%	~	33.4101	7.67%	~	27.7503
	Ours-ELG-inter	22.6303	2.99%	~	26.8971	4.08%	~	32.8841	5.97%	~	27.4705
	Ours-ELG-intra	22.6052	2.87%	~	26.8063	3.73%	~	32.6863	5.45%	~	27.3659

5.2 GENERALIZATION ANALYSIS

We further evaluate all methods on unseen larger sizes and gathered the results in Table 2. As revealed, the cross-size generalization issue of AMDKD-POMO* is more pronounced, which leads to a substantial deterioration in performance. Ours-POMO-inter surpasses POMO-random, POMO-60, POMO-100 and AMDKD-POMO across all sizes for both TSP and CVRP, and achieves competitive performance to POMO-150 (for CVRP200) and Omni-POMO (for TSP500 and CVRP500). Leveraging intra-task regularization to prioritize the learning of the latest larger sizes, Ours-POMO-intra further outperforms POMO-150 and Omni-POMO across all sizes for both TSP and CVRP. It is worth noting that Omni-POMO is trained on a broader range of sizes (including larger ones up to 200), which inherently offers Omni-POMO the potential for superior performance on larger sizes. Focusing on enhancing generalization on large problem sizes, ELG models trained on three specific sizes outperform their POMO counterparts (e.g., POMO-150 vs. ELG-150) on size 500 for both TSP and CVRP, and also exhibit significantly superior overall generalization performance in terms of average objective values across multiple problem sizes. Despite the superiority of ELG, both Ours-ELG-inter and Ours-ELG-intra still surpass ELG-60, ELG-100, ELG-150 and ELG-random across all sizes for both TSP and CVRP. Notably, Ours-ELG-intra consistently achieves lowest average objective values across the three sizes compared to all other neural baselines for both TSP and CVRP, which demonstrates the effectiveness of our approach in enhancing cross-size generalization of a backbone model.

We also extend the evaluation to well-established benchmark datasets TSPLIB (Reinelt, 1991) and CVRPLIB (Uchoa et al., 2017) with size smaller than 500. The detailed results are reported in Table 6 and Table 7, respectively, where the gaps are calculated based on the optimal solution values for the instances. POMO-60, POMO-100, AMDKD-POMO*, POMO-random, ELG-60 and ELG-100 are omitted due to their clear inferiority to POMO-150 and ELG-150 as shown in Table 1 and Table

Table 3: Generalization performance on instances ($50 \leq N \leq 500$) from benchmark instances.

	POMO-60	POMO-100	POMO-150	AMDKD-POMO	Omni-POMO	Ours-Inter
TSPLIB	9.71%	4.49%	4.18%	5.17%	3.11%	4.07%
CVRPLIB	13.59%	12.30%	9.21%	7.09%	5.83%	5.45%

2. Notably, benchmark datasets usually encompass a diverse range of sizes and customer distribution patterns. For our approach, we emphasize the intra-task regularization given its decent performance demonstrated earlier. The results show that Ours-POMO surpasses AMDKD-POMO that focuses on enhancing cross-size generalization. Although Omni-POMO is specially designed to enhance generalization across both size and distribution, our approach still delivers competitive performance to Omni-POMO. This further showcases the efficiency and effectiveness of our approach. Owing to meticulous designs tailored to bolster generalization on complex node distributions and large problem sizes, ELG-150 surpasses POMO-150 on both TSP and CVRP. Additionally, Ours-POMO and Ours-ELG outstrip their respective backbone baselines, i.e., POMO-150 and ELG-150, further demonstrating the effectiveness of our approach in enhancing cross-size generalizability (see Appendix B.1 for details).

We further extend the evaluation to realistic data taken from “World TSP”, which is available at (rea) to show that both Ours-POMO and Ours-ELG consistently surpass their respective backbone baselines, i.e., POMO-150 and ELG-150, which further showcases the effectiveness of our approach (see Appendix B.2 for details).

5.3 ABLATION STUDY

In Table 4, we conduct an ablation study to clarify the effectiveness of each component of our approach on TSP and CVRP (refer to Appendix C.1), where only one regularization scheme can be used in our approach to keep a stable update of the exemplar model. The markers “ \checkmark ” and “ \times ” denote the utilization or exclusion of the corresponding component, respectively. The gaps are calculated based on the solutions acquired by Concorde in Table 1. As exhibited, experience replay, inter-task and intra-task regularization schemes contribute to the reduction of objective values and optimality gaps across all sizes, affirming their effectiveness in enhancing cross-size generalizability. Further combining them together, both Ours-inter and Ours-intra (last two rows) achieve better performance.

We further conduct an ablation study to demonstrate the effectiveness of the proposed regularization schemes, including both the inter-task regularization scheme and the intra-task one (see Appendix C.2 for details).

We also conduct experiments to show that our approach can consistently improve the performance across diverse sizes as the training progresses. To this end, we use the obtained models after training on each size to evaluate on both seen and unseen sizes. We present the details in Appendix D.

6 CONCLUSIONS AND FUTURE WORK

This paper presents a continual learning based framework to foster the cross-size generalization of deep models for VRPs. We leverage either inter-task or intra-task regularization scheme to retain the valuable insights derived from previously trained exemplar models for facilitating subsequent training. To mitigate the catastrophic forgetting, we exploit the experience replay to revisit instances of formerly trained smaller sizes. Results show that our approach not only significantly strengthens the cross-size generalization performance, but also delivers predominantly superior performance to state-of-the-art deep models specialized for the generalizability enhancement.

Scaling up to substantially large problem instances is important for future research. Bolstered by the superior cross-size generalization capacity, we will further improve the continual learning framework to train reliable deep models for handling large-scale VRPs, e.g., in a divide-and-conquer

manner. Additionally, explicitly enhancing the cross-distribution generalization in the proposed CL framework could further unleash the potential of our approach in real-world applications.

REFERENCES

- <https://www.math.uwaterloo.ca/tsp/world/countries.html>.
- David L Applegate, Robert E Bixby, Vašek Chvátal, and William J Cook. Concorde TSP solver, 2020. URL <http://www.math.uwaterloo.ca/tsp/concorde/>.
- Barrie M Baker and MA1951066 Aye chew. A genetic algorithm for the vehicle routing problem. *Computers & Operations Research*, 30(5):787–800, 2003.
- Irwan Bello, Hieu Pham, Quoc V Le, Mohammad Norouzi, and Samy Bengio. Neural combinatorial optimization with reinforcement learning. In *International Conference on Machine Learning (Workshop)*, 2017.
- Yoshua Bengio, Andrea Lodi, and Antoine Prouvost. Machine learning for combinatorial optimization: a methodological tour d’horizon. *European Journal of Operational Research*, 290(2):405–421, 2021.
- Jieyi Bi, Yining Ma, Jiahai Wang, Zhiguang Cao, Jinbiao Chen, Yuan Sun, and Yeow Meng Chee. Learning generalizable models for vehicle routing problems via knowledge distillation. In *Advances in Neural Information Processing Systems*, volume 35, pp. 31226–31238, 2022.
- Zhiyuan Chen and Bing Liu. *Lifelong machine learning*, volume 1. Springer, 2018.
- Matthias De Lange, Rahaf Aljundi, Marc Masana, Sarah Parisot, Xu Jia, Aleš Leonardis, Gregory Slabaugh, and Tinne Tuytelaars. A continual learning survey: Defying forgetting in classification tasks. *IEEE Transactions on Pattern Analysis and Machine Intelligence*, 44(7):3366–3385, 2021.
- Robert M French. Catastrophic forgetting in connectionist networks. *Trends in Cognitive Sciences*, 3(4):128–135, 1999.
- Zhang-Hua Fu, Kai-Bin Qiu, and Hongyuan Zha. Generalize a small pre-trained model to arbitrarily large tsp instances. In *Proceedings of the AAAI Conference on Artificial Intelligence*, volume 35, pp. 7474–7482, 2021.
- Chengrui Gao, Haopu Shang, Ke Xue, Dong Li, and Chao Qian. Towards generalizable neural solvers for vehicle routing problems via ensemble with transferrable local policy. In *International Joint Conference on Artificial Intelligence*, 2023.
- Raia Hadsell, Dushyant Rao, Andrei A Rusu, and Razvan Pascanu. Embracing change: Continual learning in deep neural networks. *Trends in Cognitive Sciences*, 24(12):1028–1040, 2020.
- Rujun Han, Xiang Ren, and Nanyun Peng. Econet: Effective continual pretraining of language models for event temporal reasoning. In *Proceedings of the 2021 Conference on Empirical Methods in Natural Language Processing*, pp. 5367–5380, 2021.
- Jiangpeng He and Fengqing Zhu. Online continual learning for visual food classification. In *Proceedings of the IEEE/CVF International Conference on Computer Vision*, pp. 2337–2346, 2021.
- Keld Helsgaun. An extension of the lin-kernighan-helsgaun tsp solver for constrained traveling salesman and vehicle routing problems. *Roskilde: Roskilde University*, 2017.
- André Hottung, Yeong-Dae Kwon, and Kevin Tierney. Efficient active search for combinatorial optimization problems. In *International Conference on Learning Representations*, 2021.
- Qingchun Hou, Jingwei Yang, Yiqiang Su, Xiaoqing Wang, and Yuming Deng. Generalize learned heuristics to solve large-scale vehicle routing problems in real-time. In *The Eleventh International Conference on Learning Representations*, 2022.

- Yuan Jiang, Yaxin Wu, Zhiguang Cao, and Jie Zhang. Learning to solve routing problems via distributionally robust optimization. In *Proceedings of the AAAI Conference on Artificial Intelligence*, 2022.
- Chaitanya K Joshi, Thomas Laurent, and Xavier Bresson. An efficient graph convolutional network technique for the travelling salesman problem. arxiv preprint arxiv: 1906.01227, 2019.
- Detian Kong, Yining Ma, Zhiguang Cao, Tianshu Yu, and Jianhua Xiao. Efficient neural collaborative search for pickup and delivery problems. *IEEE Transactions on Pattern Analysis and Machine Intelligence*, 2024.
- Wouter Kool, Herke van Hoof, and Max Welling. Attention, learn to solve routing problems! In *International Conference on Learning Representations*, 2018.
- Bernhard H Korte, Jens Vygen, B Korte, and J Vygen. *Combinatorial optimization*, volume 1. Springer, 2011.
- Yeong-Dae Kwon, Jinho Choo, Byoungjip Kim, Iljoo Yoon, Youngjune Gwon, and Seungjai Min. POMO: Policy optimization with multiple optima for reinforcement learning. In *Advances in Neural Information Processing Systems*, volume 33, pp. 21188–21198, 2020.
- Jan Karel Lenstra and AHG Rinnooy Kan. Complexity of vehicle routing and scheduling problems. *Networks*, 11(2):221–227, 1981.
- Jingwen Li, Yining Ma, Ruize Gao, Zhiguang Cao, Andrew Lim, Wen Song, and Jie Zhang. Deep reinforcement learning for solving the heterogeneous capacitated vehicle routing problem. *IEEE Transactions on Cybernetics*, 52(12):13572–13585, 2021a.
- Jingwen Li, Liang Xin, Zhiguang Cao, Andrew Lim, Wen Song, and Jie Zhang. Heterogeneous attentions for solving pickup and delivery problem via deep reinforcement learning. *IEEE Transactions on Intelligent Transportation Systems*, 2021b.
- Jingwen Li, Yining Ma, Zhiguang Cao, Yaxin Wu, Wen Song, Jie Zhang, and Yeow Meng Chee. Learning feature embedding refiner for solving vehicle routing problems. *IEEE Transactions on Neural Networks and Learning Systems*, 2023.
- Sirui Li, Zhongxia Yan, and Cathy Wu. Learning to delegate for large-scale vehicle routing. In *Advances in Neural Information Processing Systems*, volume 34, pp. 26198–26211, 2021c.
- Zhizhong Li and Derek Hoiem. Learning without forgetting. *IEEE Transactions on Pattern Analysis and Machine Intelligence*, 40(12):2935–2947, 2017.
- Michal Lisicki, Arash Afkanpour, and Graham W Taylor. Evaluating curriculum learning strategies in neural combinatorial optimization. *arXiv preprint arXiv:2011.06188*, 2020.
- Arun Mallya and Svetlana Lazebnik. Packnet: Adding multiple tasks to a single network by iterative pruning. In *Proceedings of the IEEE conference on Computer Vision and Pattern Recognition*, pp. 7765–7773, 2018.
- Umberto Michieli and Pietro Zanuttigh. Incremental learning techniques for semantic segmentation. In *Proceedings of the IEEE/CVF International Conference on Computer Vision (Workshop)*, pp. 0–0, 2019.
- Mohammadreza Nazari, Afshin Oroojlooy, Martin Takáč, and Lawrence V Snyder. Reinforcement learning for solving the vehicle routing problem. In *Advances in Neural Information Processing Systems*, pp. 9861–9871, 2018.
- German I Parisi, Ronald Kemker, Jose L Part, Christopher Kanan, and Stefan Wermter. Continual lifelong learning with neural networks: A review. *Neural Networks*, 113:54–71, 2019.
- Ruizhong Qiu, Zhiqing Sun, and Yiming Yang. Dimes: A differentiable meta solver for combinatorial optimization problems. *Advances in Neural Information Processing Systems*, 35:25531–25546, 2022.

- Sylvestre-Alvise Rebuffi, Alexander Kolesnikov, Georg Sperl, and Christoph H Lampert. icarl: Incremental classifier and representation learning. In *Proceedings of the IEEE Conference on Computer Vision and Pattern Recognition*, pp. 2001–2010, 2017.
- Gerhard Reinelt. TSPLIB-A traveling salesman problem library. *ORSA Journal on Computing*, 3(4):376–384, 1991.
- David Rolnick, Arun Ahuja, Jonathan Schwarz, Timothy Lillicrap, and Gregory Wayne. Experience replay for continual learning. *Advances in Neural Information Processing Systems*, 32, 2019.
- Michael Schneider, Andreas Stenger, and Dominik Goeke. The electric vehicle-routing problem with time windows and recharging stations. *Transportation Science*, 48(4):500–520, 2014.
- Yuan Sun, Xiaodong Li, and Andreas Ernst. Using statistical measures and machine learning for graph reduction to solve maximum weight clique problems. *IEEE transactions on pattern analysis and machine intelligence*, 43(5):1746–1760, 2019.
- Zhiqing Sun and Yiming Yang. Difusco: Graph-based diffusion solvers for combinatorial optimization. *arXiv preprint arXiv:2302.08224*, 2023.
- Eduardo Uchoa, Diego Pecin, Artur Pessoa, Marcus Poggi, Thibaut Vidal, and Anand Subramanian. New benchmark instances for the capacitated vehicle routing problem. *European Journal of Operational Research*, 257(3):845–858, 2017.
- Ashish Vaswani, Noam Shazeer, Niki Parmar, Jakob Uszkoreit, Llion Jones, Aidan N Gomez, Łukasz Kaiser, and Illia Polosukhin. Attention is all you need. In *Advances in neural information processing systems*, pp. 5998–6008, 2017.
- Thibaut Vidal. Hybrid genetic search for the cvrp: Open-source implementation and swap* neighborhood. *Computers & Operations Research*, 140:105643, 2022.
- Oriol Vinyals, Meire Fortunato, and Navdeep Jaitly. Pointer networks. In *Advances in Neural Information Processing Systems*, volume 28, pp. 2692–2700, 2015.
- Ronald J Williams. Simple statistical gradient-following algorithms for connectionist reinforcement learning. *Machine learning*, 8:229–256, 1992.
- Yaoxin Wu, Wen Song, Zhiguang Cao, Jie Zhang, and Andrew Lim. Learning improvement heuristics for solving routing problems. *IEEE Transactions on Neural Networks and Learning Systems*, 2021.
- Liang Xin, Wen Song, Zhiguang Cao, and Jie Zhang. Multi-decoder attention model with embedding glimpse for solving vehicle routing problems. In *AAAI Conference on Artificial Intelligence*, 2020.
- Cong Zhang, Yaoxin Wu, Yining Ma, Wen Song, Zhang Le, Zhiguang Cao, and Jie Zhang. A review on learning to solve combinatorial optimisation problems in manufacturing. *IET Collaborative Intelligent Manufacturing*, 5(1):e12072, 2023a.
- Dongxiang Zhang, Ziyang Xiao, Yuan Wang, Mingli Song, and Gang Chen. Neural tsp solver with progressive distillation. In *Proceedings of the AAAI Conference on Artificial Intelligence*, volume 37, pp. 12147–12154, 2023b.
- Jianan Zhou, Yaoxin Wu, Wen Song, Zhiguang Cao, and Jie Zhang. Towards omni-generalizable neural methods for vehicle routing problems. In *the 40th International Conference on Machine Learning (ICML 2023)*, 2023.
- Zefang Zong, Hansen Wang, Jingwei Wang, Meng Zheng, and Yong Li. Rbg: Hierarchically solving large-scale routing problems in logistic systems via reinforcement learning. In *Proceedings of the 28th ACM SIGKDD Conference on Knowledge Discovery and Data Mining*, pp. 4648–4658, 2022.

A FULL RESULTS ON TSP AND CVRP (SEEN SCALES)

In Table 1, regarding the learning-oriented methods, we mainly displayed their results yielded with the data augmentation strategy (A). Here we show the full results with (A) and without (N) the data augmentation in Table 5. As shown, the inference time without data augmentation is significantly shorter than that with data augmentation. On the other hand, it is clear that both Ours-inter and Ours-intra achieve the best average performance among all deep models, no matter the data augmentation strategy is used or not.

Method	Test on N=60			Test on N=100			Test on N=150			Average of Total costs	
	Obj.	Gap	Time	Obj.	Gap	Time	Obj.	Gap	Time		
TSP	Concorde	6.1729	-	(7m)	7.7646	-	(1.7h)	9.3462	-	(22m)	7.7612
	LKH3	6.1729	0.00%	(14m)	7.7646	0.00%	(9.8h)	9.3462	0.00%	(2.1h)	7.7612
	(N) AMDKD-POMO*	6.2115	0.62%	6s	7.8312	0.86%	15s	9.5229	1.89%	4s	7.8552
	(N) POMO-60	6.1811	0.13%	~	7.8514	1.12%	~	9.7019	3.81%	~	7.9115
	(N) POMO-100	6.1972	0.39%	~	7.7908	0.34%	~	9.4500	1.11%	~	7.8160
	(N) POMO-150	6.3031	2.11%	~	7.8702	1.36%	~	9.3866	0.43%	~	7.8533
	(N) POMO-random	6.2007	0.45%	~	7.8027	0.49%	~	9.4443	1.05%	~	7.8159
	(N) AMDKD-POMO	6.2076	0.56%	~	7.8292	0.83%	~	9.5035	1.68%	~	7.8468
	(N) Omni-POMO [†]	6.3065	2.16%	5s	7.9425	2.29%	18s	9.5795	2.50%	5s	7.9428
	(N) Ours-inter	6.1882	0.25%	6s	7.8007	0.47%	15s	9.4275	0.87%	4s	7.8055
	(N) Ours-intra	6.1889	0.26%	~	7.7995	0.45%	~	9.4010	0.59%	~	7.7965
	(A) AMDKD-POMO*	6.1828	0.16%	36s	7.7930	0.37%	2m	9.4539	1.15%	33s	7.8092
	(A) POMO-60	6.1746	0.03%	~	7.8050	0.52%	~	9.5909	2.62%	~	7.8568
	(A) POMO-100	6.1768	0.06%	~	7.7753	0.14%	~	9.3987	0.56%	~	7.7836
	(A) POMO-150	6.1928	0.32%	~	7.7875	0.30%	~	9.3812	0.36%	~	7.7868
CVRP	(A) POMO-random	6.1778	0.08%	~	7.7782	0.18%	~	9.3937	0.51%	~	7.7832
	(A) AMDKD-POMO	6.1820	0.15%	~	7.7916	0.35%	~	9.4473	1.08%	~	7.8070
	(A) Omni-POMO [†]	6.2351	1.01%	34s	7.8650	1.29%	2.5m	9.4958	1.60%	37s	7.8653
	(A) Ours-inter	6.1758	0.05%	36s	7.7775	0.17%	2m	9.3883	0.45%	33s	7.7805
	(A) Ours-intra	6.1758	0.05%	~	7.7764	0.15%	~	9.3820	0.38%	~	7.7781
	HGS	11.9471	-	(15.3h)	15.5642	-	(25.6h)	19.0554	-	(6.2h)	15.5222
	LKH3	11.9694	0.19%	(3.5d)	15.6473	0.53%	(6.5d)	19.2208	0.87%	(13h)	15.6125
	(N) AMDKD-POMO*	12.5745	5.25%	7s	15.9485	2.47%	22s	20.0788	5.37%	6s	16.2006
	(N) POMO-60	12.1757	1.91%	~	16.3058	4.77%	~	20.5332	7.76%	~	16.3382
	(N) POMO-100	12.4140	3.91%	~	15.8369	1.75%	~	19.8641	4.24%	~	16.0383
	(N) POMO-150	12.7088	6.38%	~	16.0346	3.02%	~	19.4822	2.24%	~	16.0752
	(N) POMO-random	12.4548	4.25%	~	15.9237	2.31%	~	19.7185	3.48%	~	16.0323
	(N) AMDKD-POMO	12.2731	2.73%	~	15.9498	2.48%	~	19.6619	3.18%	~	15.9616
	(N) Omni-POMO [†]	12.4879	4.53%	6s	16.1511	3.77%	20s	19.7527	3.66%	6s	16.1505
	(N) Ours-inter	12.1818	1.97%	7s	15.9166	2.26%	22s	19.5555	2.62%	6s	15.8846
	(N) Ours-intra	12.1838	1.98%	~	15.9093	2.22%	~	19.5342	2.51%	~	15.8758
	(A) AMDKD-POMO*	12.3561	3.42%	56s	15.8854	2.06%	3m	19.8395	4.12%	33s	16.0270
	(A) POMO-60	12.0656	0.99%	~	16.0914	3.39%	~	20.2573	6.31%	~	16.1381
	(A) POMO-100	12.2531	2.56%	~	15.7544	1.22%	~	19.6856	3.31%	~	15.8977
	(A) POMO-150	12.4322	4.06%	~	15.8924	2.11%	~	19.3683	1.64%	~	15.8976
	(A) POMO-random	12.2758	2.75%	~	15.7942	1.48%	~	19.6121	2.92%	~	15.8940
	(A) AMDKD-POMO	12.1487	1.69%	~	15.8119	1.72%	~	19.5280	2.48%	~	15.8362
	(A) Omni-POMO [†]	12.2996	2.95%	45s	15.9878	2.72%	2.5m	19.5975	2.85%	45s	15.9616
	(A) Ours-inter	12.0660	1.00%	56s	15.7848	1.42%	3m	19.4109	1.87%	33s	15.7539
	(A) Ours-intra	12.0663	1.00%	~	15.7781	1.37%	~	19.3938	1.78%	~	15.7461

Bold and *italics* refer to the best and the second-best performance, respectively, among all deep models.

~ The inference time of a method is equal to that of the preceding method in the row above, since those deep models except for Omni-POMO utilize the original POMO architecture and result in the same inference efficiency.

[†] The training size range of Omni-POMO is [50, 200], which is broader than our [60, 150].

Table 5: Comparison results on TSP and CVRP (seen scales).

B DETAILED GENERALIZATION RESULTS ON BENCHMARK DATASETS.

B.1 RESULTS ON TSPLIB AND CVRPLIB

We evaluate all methods on the classic benchmark datasets, including TSPLIB (Reinelt, 1991) and CVRPLIB (Uchoa et al., 2017), in which we choose representative instances with size $N \in [50, 500]$. Note that both benchmark datasets encompass a diverse range of sizes and distributions.

The detailed results are shown in Table 6 and Table 7, where the gaps are calculated based on the optimal solution values for the instances. From two tables, we observe that our approach outperforms AMDKD-POMO and all POMO models trained on specific sizes on both benchmark datasets. Note that Omni-POMO is explicitly specialized for improving generalization across both size and distribution, which has the potential to achieve desirable performance on benchmark datasets whose instances encompass a diverse range of sizes and distributions. More specific, the setting that explicitly training with more diverse sizes and distributions, will inherently favor Omni-POMO over our approach. Whereas, our approach still yields competitive performance in comparison against Omni-POMO, e.g., with the average gap of 5.45% (Ours) VS. 5.83% (Omni-POMO) on CVRPLIB, which further underscores the effectiveness of our approach.

Table 6: Detailed generalization results on instances from TSPLIB.

Instance	Opt.	POMO-60		POMO-100		POMO-150		AMDKD-POMO	Omni-POMO [‡]		Ours
		Obj.	Gap	Obj.	Gap	Obj.	Gap	Obj.	Gap	Obj.	Gap
berlin52	7544	7544	0.00%	7545	0.01%	7613	0.92%	7545	0.01%	8003	6.08%
st70	675	677	0.30%	677	0.30%	678	0.44%	677	0.30%	680	0.74%
eil76	538	547	1.67%	544	1.12%	549	2.05%	550	3.77%	557	3.53%
rd100	7910	7920	0.13%	7910	0.00%	7952	0.53%	7934	0.30%	7958	0.61%
KroA100	21282	21786	2.34%	21667	1.81%	21596	1.48%	22077	3.74%	21305	0.11%
KroB100	22141	22941	3.61%	22370	1.03%	22575	1.96%	22745	2.73%	22650	2.30%
lin105	14379	14808	2.98%	14557	1.24%	14808	2.98%	14898	3.61%	14819	3.06%
pr124	59030	59031	0.00%	59388	0.61%	59595	0.96%	59521	0.83%	59238	0.35%
ch130	6110	6188	1.28%	6133	0.38%	6142	0.52%	6159	0.80%	6251	2.31%
pr136	96772	100459	38.12%	97540	0.80%	97668	0.93%	97951	1.22%	97780	1.04%
gr137	699	746	6.72%	755	8.01%	759	8.58%	773	10.59%	772	10.44%
ch150	6528	6679	2.31%	6559	0.48%	6579	0.78%	6583	0.82%	6586	0.89%
KroA200	29368	31819	8.35%	30415	3.57%	30015	2.20%	30672	4.44%	29823	1.55%
KroB200	29437	32020	8.78%	30880	4.90%	30172	2.50%	30990	5.28%	29814	1.28%
ts225	126643	135704	7.16%	130990	3.43%	128045	1.14%	128911	1.79%	128770	1.68%
a280	2579	3101	20.24%	2951	0.45%	2788	8.10%	2809	8.92%	2695	4.50%
rd400	15281	18055	18.15%	17342	13.49%	16155	5.72%	16160	5.75%	15948	4.37%
fl417	11861	14319	20.72%	14396	21.37%	14225	19.93%	14004	18.07%	12683	6.93%
pcb442	50778	71914	41.62%	62145	22.39%	54683	7.69%	63643	25.34%	59761	17.69%
Avg. Gap	0.00%	-	9.71%	-	4.49%	-	4.18%	-	5.17%	-	3.11%
											4.07%

Table 7: Detailed generalization results on instances from CVRPLIB.

Instance	Opt.	POMO-60		POMO-100		POMO-150		AMDKD-POMO	Omni-POMO [‡]		Ours
		Obj.	Gap	Obj.	Gap	Obj.	Gap	Obj.	Gap	Obj.	Gap
A-n53-k7	1010	1315	30.20%	1318	30.50%	1152	14.06%	1111	10.00%	1105	9.41%
A-n60-k9	1354	1741	28.58%	1739	28.43%	1657	22.38%	1574	16.25%	1465	8.20%
A-n80-k10	1763	2692	52.69%	2740	55.42%	2816	59.73%	2136	21.16%	2127	20.65%
X-n101-k25	27591	29786	7.96%	29287	6.15%	29398	6.55%	29306	6.22%	29442	6.71%
X-n10-k13	14971	15530	3.73%	15161	1.27%	15130	1.06%	15202	1.54%	15285	2.10%
X-n120-k6	13332	14239	6.80%	14570	9.29%	14060	5.46%	14010	5.09%	13944	4.59%
X-n129-k18	28940	30154	4.20%	29569	2.17%	29343	1.39%	29702	2.63%	29975	3.58%
X-n139-k10	13590	14269	5.00%	14080	3.61%	13855	1.95%	13890	2.21%	14019	3.16%
X-n148-k46	43448	46146	6.21%	47621	9.61%	45850	5.53%	46451	6.91%	46438	6.88%
X-n157-k13	16876	17663	4.66%	18302	8.45%	18340	8.68%	17523	3.83%	17107	1.37%
X-n167-k10	20557	22306	8.51%	21297	3.60%	20995	2.13%	21068	2.49%	21436	4.28%
X-n190-k8	16980	18757	10.47%	18164	6.97%	18140	6.83%	18169	7.00%	17645	3.92%
X-n200-k36	58578	62737	7.10%	61933	5.73%	61397	4.81%	61384	4.79%	61496	4.98%
X-n251-k28	38684	42430	9.69%	41360	6.92%	40024	3.47%	40595	4.94%	40059	3.55%
X-n298-k31	34231	38749	13.20%	38611	12.80%	35663	4.18%	37221	8.74%	36384	6.29%
X-n351-k40	25896	30289	16.96%	28343	9.45%	27952	7.94%	28315	9.34%	27515	6.25%
X-n401-k29	66154	72209	9.15%	71173	7.59%	69641	5.27%	69227	4.65%	68234	3.14%
X-n449-k29	55233	63569	15.09%	61915	12.08%	58418	5.77%	59929	8.50%	58037	5.08%
X-n491-k59	66483	78463	18.02%	75620	13.74%	71668	7.80%	72087	8.43%	70923	6.68%
Avg. Gap	0.00%	-	13.59%	-	12.30%	-	9.21%	-	7.09%	-	5.83%
											5.45%

B.2 RESULTS ON WORLD TSP

In Table 8, we further extend the evaluation to realistic data taken from “World TSP”, which is available at (rea). Specifically, we randomly sample instances from the map across three unseen sizes during training, (i.e., 200, 300, and 500, with 128 instances for each), from 3 different countries (i.e., Uruguay, Egypt and Ireland). Each instance is normalized to a $[0, 1]$ square, and the optimality gaps are calculated based on the solutions generated by Concorde solver. We compare our approach (i.e., Ours-POMO-intra and Ours-ELG-intra) with POMO-150, AMDKD-POMO, Omni-POMO and ELG-150, given their robust performance demonstrated in prior evaluations. The results

show that Ours-POMO outstrips all other POMO-based baseline methods across all sizes and countries, despite the fact that Omni-POMO is specially designed for enhanced generalization across both size and distribution. Furthermore, both Ours-POMO and Ours-ELG consistently surpass their respective backbone baselines, i.e., POMO-150 and ELG-150, which further showcases the effectiveness of our approach.

Table 8: Generalization results on real-world TSP instances in 3 different countries (i.e., Uruguay, Egypt and Ireland).

Method	N=200		N=300		N=500		
	Obj.	Gap	Obj.	Gap	Obj.	Gap	
UY734	Concorde	6.7661	-	7.6513	-	9.5436	-
	AMDKD-POMO	6.9832	3.21%	8.1043	5.92%	10.7382	12.52%
	Omni-POMO	6.9171	2.23%	7.9659	4.11%	10.5126	10.15%
	POMO-150	6.9349	2.50%	7.9509	3.92%	10.5336	10.37%
	Ours-POMO-intra	6.8817	1.71%	7.8522	2.63%	10.3176	8.11%
	ELG-150	6.9125	2.16%	7.8661	2.81%	10.1942	6.82%
	Ours-ELG-intra	6.8495	1.23%	7.8480	2.57%	10.1730	6.60%
EG7146	Concorde	6.8792	-	7.7689	-	10.0568	-
	AMDKD-POMO	7.1246	3.57%	8.1889	5.41%	11.3192	12.55%
	Omni-POMO	7.0456	2.42%	8.1475	4.87%	11.1304	10.68%
	POMO-150	7.0546	2.55%	8.1218	4.54%	11.1117	10.49%
	Ours-POMO-intra	7.0130	1.95%	7.9952	2.91%	10.8818	8.20%
	ELG-150	7.0924	3.10%	8.0226	3.27%	10.8213	7.60%
	Ours-ELG-intra	7.0107	1.91%	7.9825	2.75%	10.7541	6.93%
EI8246	Concorde	7.0635	-	8.0201	-	10.2078	-
	AMDKD-POMO	7.3670	4.30%	8.5288	6.34%	11.5648	13.29%
	Omni-POMO	7.2734	2.97%	8.4244	5.04%	11.3692	11.38%
	POMO-150	7.2739	3.00%	8.4164	4.94%	11.3528	11.22%
	Ours-POMO-intra	7.2473	2.60%	8.2936	3.41%	11.1176	8.91%
	ELG-150	7.3260	3.72%	8.2643	3.05%	10.9422	7.20%
	Ours-ELG-intra	7.2360	2.44%	8.2441	2.79%	10.9201	6.98%

C MORE ABLATION STUDY RESULTS

C.1 ABLATION STUDY ON COMPONENTS OF OUR APPROACH FOR CVRP

In Table 4, we display the ablation study on the effectiveness of each component of our approach for TSP. Here we show the corresponding results for CVRP in Table 9. As revealed, experience replay, inter-task and intra-task regularization schemes contribute to the reduction of objective values and optimality gaps across all sizes, affirming their effectiveness in enhancing cross-size generalizability. Further combining experience replay and regularization scheme together, both Ours-inter and Ours-intra (last two rows) achieve better performance.

Table 9: Ablation study on CVRP.

ER	Inter-task	Intra-task	N=60		N=100		N=150	
			Obj.	Gap	Obj.	Gap	Obj.	Gap
×	×	×	12.1174	1.43%	15.8528	1.86%	19.5024	2.35%
×	✓	×	12.0829	1.14%	15.8109	1.59%	19.4472	2.06%
×	×	✓	12.0855	1.16%	15.8085	1.57%	19.4289	1.96%
✓	×	×	12.0786	1.10%	15.8187	1.64%	19.4389	2.01%
✓	✓	×	12.0660	1.00%	15.7848	1.42%	19.4109	1.87%
✓	×	✓	12.0663	1.00%	15.7781	1.37%	19.3938	1.78%

C.2 ABLATION STUDY ON REGULARIZATION SCHEMES

To verify the effectiveness of the regularization schemes designed in our approach, we further analyze the evaluation results of our accomplished models after training on each size with inter-task regularization scheme, intra-task regularization scheme, and without regularization scheme, across three sizes (i.e., 60, 100 and 150) for both TSP and CVRP. The corresponding curves are depicted in Figure 3 and Figure 4, respectively, where we also present the average objective values across

those sizes, in order to show the overall improved cross-size generalization performance. As revealed, both inter-task and intra-task regularization schemes accelerate the learning efficiency and boost the overall results in comparison with the one without regularization scheme for both TSP and CVRP, which showcases the effectiveness of the proposed regularization schemes. Moreover, inter-task regularization scheme is superior to the intra-task one in terms of the learning efficiency on smaller sizes (i.e., 60), while the other way round on larger sizes (i.e., 100 and 150). This is reasonable since the intra-task regularization scheme concentrate more on efficiently learning the latest larger sizes. Furthermore, the intra-task achieves the fastest learning efficiency and the lowest objective value when averaging the objective values across all three sizes.

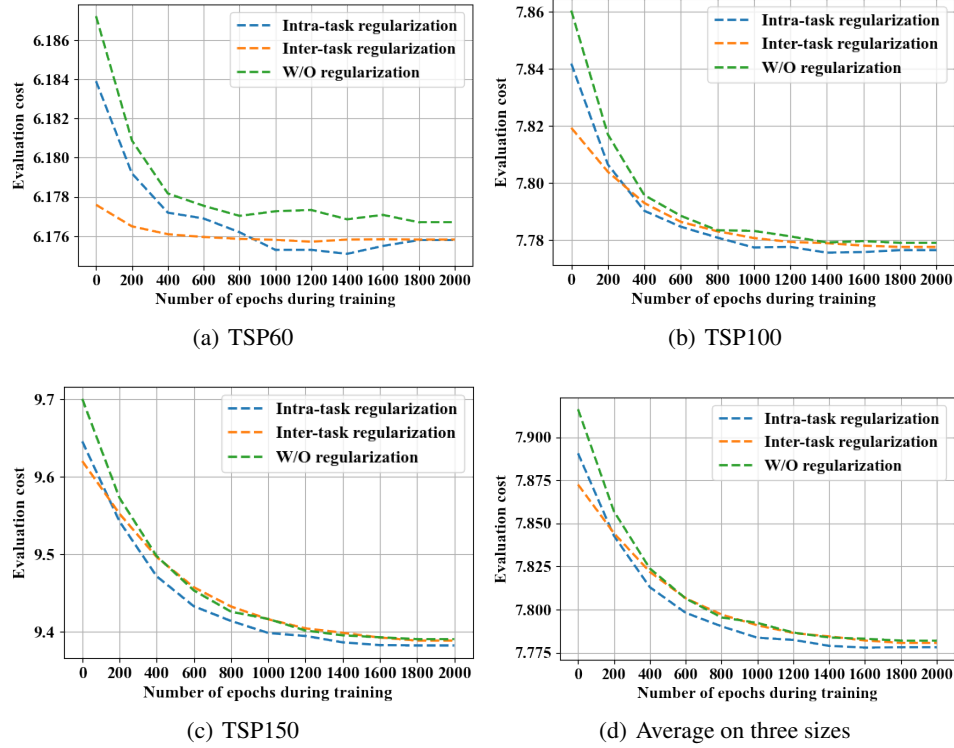


Figure 3: Curves of learning progress for our approach on TSP.

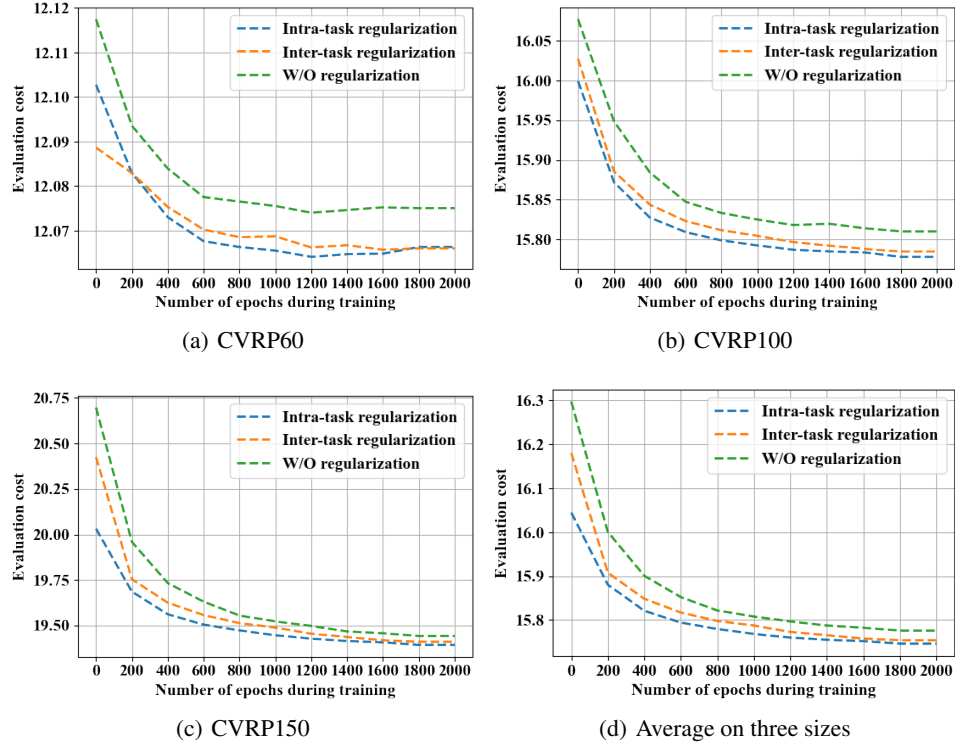


Figure 4: Curves of learning progress for our approach on CVRP.

Table 10: Validation results on seen and unseen sizes.

Method	Test on N=100		Test on N=150		Test on N=200		
	Obj.	Gap	Obj.	Gap	Obj.	Gap	
TSP	Ours (after training on 60)	7.8419	1.00%	9.6460	3.21%	11.2975	5.90%
	Ours (after training on 70)	7.8065	0.54%	9.5426	2.10%	11.1413	4.43%
	Ours (after training on 80)	7.7902	0.33%	9.4715	1.34%	11.0082	3.19%
	Ours (after training on 90)	7.7846	0.26%	9.4327	0.93%	10.9116	2.28%
	Ours (after training on 100)	7.7808	0.21%	9.4137	0.72%	10.8585	1.78%
	Ours (after training on 110)	7.7773	0.16%	9.3982	0.56%	10.8029	1.26%
	Ours (after training on 120)	7.7775	0.17%	9.3943	0.52%	10.7880	1.12%
	Ours (after training on 130)	7.7755	0.14%	9.3861	0.43%	10.7629	0.89%
	Ours (after training on 140)	7.7757	0.14%	9.3824	0.39%	10.7526	0.79%
	Ours (after training on 150)	7.7764	0.15%	9.3820	0.38%	10.7445	0.71%
CVRP	Ours (after training on 60)	15.9992	2.23%	20.0320	4.22%	23.5642	6.08%
	Ours (after training on 70)	15.8721	1.42%	19.6862	2.42%	23.0514	3.77%
	Ours (after training on 80)	15.8275	1.13%	19.5619	1.78%	22.8025	2.65%
	Ours (after training on 90)	15.8092	1.02%	19.5051	1.48%	22.7007	2.19%
	Ours (after training on 100)	15.7987	0.95%	19.4732	1.31%	22.6235	1.84%
	Ours (after training on 110)	15.7924	0.91%	19.4466	1.18%	22.5745	1.62%
	Ours (after training on 120)	15.7870	0.88%	19.4282	1.08%	22.5361	1.45%
	Ours (after training on 130)	15.7849	0.86%	19.4148	1.01%	22.4948	1.26%
	Ours (after training on 140)	15.7835	0.85%	19.4075	0.97%	22.4695	1.15%
	Ours (after training on 150)	15.7781	0.82%	19.3938	0.90%	22.4436	1.03%

D VALIDATION ON BOTH SEEN AND UNSEEN SIZES

We evaluate the obtained models after training on each size with intra-task regularization scheme. On both seen and unseen sizes, i.e., 100, 150 and 200, these models are evaluated to showcase that our approach can consistently improve the performance of the deep model, as the training progresses.

The results are summarized in Table 10, where the gaps are calculated based on the solutions acquired by Concorde for TSP and HGS for CVRP in Table 1. We observe that when we evaluate the models on size 100, it progressively reduces the gaps before the training process reaching size 100. Furthermore, it effectively retains the acquired knowledge and superiority on size 100, after further trained on instances with larger sizes. The models trained after size 100 still show decreasing gaps on size 100. Similarly, in the case of testing on the larger sizes, i.e., 150 and 200, our approach consistently enhances the performance during the whole training phase. These findings highlight that our approach excels not only in preserving superior performance on small sizes but also in consistently enhancing performance on larger sizes.

E DETAILS OF POMO MODEL.

POMO uses the encoder-decoder structure to sequentially construct solutions for VRPs. Specifically, the encoder projects problem-specific features into high-dimensional node embeddings for informative representation learning. Afterwards, the decoder sequentially constructs a solution $\tau = \{\tau_1, \tau_2, \dots, \tau_{T_c}\}$ with T_c steps for a VRP instance of problem size N , conditioned on the node embeddings and partial tour at each step. Specifically, $T_c = N$ for TSP, and $T_c \geq N$ for CVRP as the depot node could be visited multiple times.

E.1 THE ENCODER

The encoder first embeds problem-specific features to higher-dimensional space, then passes them to stacked attention layers to extract useful information for better representation. The problem-specific features of node $v_i, i \in \{1, 2, \dots, N\}$ contain 2-dimensional location coordinates (for both TSP and CVRP) and 1-dimensional demand vector (for CVRP only), which are linearly projected to initial node embedding h_i^0 of 128-dimension [1]. Then they are processed through $L = 6$ attention layers with different parameters to derive the final node embedding h_i^L , where each attention layer is composed of a multi-head attention (MHA) sub-layer and a feed-forward (FF) sub-layer. Following the original design of the Transformer architecture [2], both the outputs of the MHA sub-layer and the FF sub-layer are followed by a skip-connection layer [3] and a batch normalization (BN) layer [4] as below,

$$\tilde{h}_i = \text{BN}(h_i^l + \text{MHA}(h_i^l)), \quad (6)$$

$$h_i^{l+1} = \text{BN}(\tilde{h}_i + \text{FF}(\tilde{h}_i)). \quad (7)$$

MHA sub-layer. The MHA sub-layer employs a multi-head self-attention mechanism [2] with $M = 8$ heads to compute the attention weights between each two nodes. Specifically, the *query/key/value* proposed in [2] are defined with $d_k = d/M$ dimension as below,

$$q_i^{l,m} = W_Q^{l,m} h_i^l, \quad k_i^{l,m} = W_K^{l,m} h_i^l, \quad v_i^{l,m} = W_V^{l,m} h_i^l. \quad (8)$$

Then the attention weights are computed by using the Softmax activation function to represent the correlation between each two nodes as follows,

$$u_{ij}^{l,m} = \text{Softmax} \left(\frac{(q_i^{l,m})^\top (k_j^{l,m})}{\sqrt{d_k}} \right). \quad (9)$$

Finally, the l -th MHA sub-layer first computes the new context vectors by performing an element-wise multiplication of the attention weights with *value*, and then aggregates the information from M heads as follows,

$$h_i^{l,m} = \sum_j u_{ij}^{l,m} v_j^{l,m}, \quad m = 1, 2, \dots, M, \quad (10)$$

$$\text{MHA}(h_i^l) = [h_i^{l,1}; h_i^{l,2}; \dots; h_i^{l,M}] W_O^l, \quad (11)$$

where $W_Q^{l,m}, W_K^{l,m}, W_V^{l,m} \in \mathbb{R}^{d \times d_k}$, $W_O^l \in \mathbb{R}^{md_k \times d}$ are learnable parameters, and $[;]$ denotes the concatenate operator.

FF sub-layer. The FF sub-layer processes the node embeddings $\tilde{h}_i, i \in \{1, 2, \dots, N\}$ through a hidden sub-layer with dimension 512 and a ReLU activation function, as follows,

$$\text{FF}(\tilde{h}_i) = W_F^1 \text{ReLU}(W_F^0 \tilde{h}_i + b_F^0) + b_F^1, \quad (12)$$

where $W_F^0, W_F^1, b_F^0, b_F^1$ are trainable parameters. At the end, the encoder outputs a set of node embeddings in the L -th layer $h_i^L, i \in \{1, 2, \dots, N\}$. These embeddings will be preserved as a part of the input to the decoder for route construction.

E.2 THE DECODER

Taking TSP as an example, the decoder first calculates the mean of node embeddings to derive the global graph embedding, i.e., $\bar{h} = \frac{1}{N} \sum_i^N h_i^L$, then defines a context vector as the combination of the graph embedding, the embeddings of the first node of the route and the last visited node. For step $t_c = 1$, we use learned parameters v^1 and v^2 as input placeholders. Note that POMO constructs N solutions by taking each of the N nodes as the first node to visit (i.e., $h_{\tau_1}^i = h_i$). Particularly, it defines N context vectors $h_i^c, \forall i \in \{1, 2, \dots, N\}$ as follows,

$$h_i^c = \begin{cases} (\bar{h}, h_i, h_{\tau_{t_c-1}}^i), & \text{if } t_c > 1 \\ (\bar{h}, v^1, v^2), & \text{if } t_c = 1 \end{cases} \quad (13)$$

where $h_{\tau_{t_c}}^i$ is the node embedding of the node visited at decoding step t_c for the i th solution. The context vectors are then processed by a MHA layer as introduced above to generate N glimpse vectors $h_i^g, i \in \{1, 2, \dots, N\}$ in parallel,

$$h_i^g = \text{MHA}(W_Q^g h_i^c, W_K^g h, W_V^g h), \quad i \in \{1, 2, \dots, N\}, \quad (14)$$

after which the decoder computes the compatibility between the enhanced glimpses and node embeddings. Then it further calculates the probabilities of selecting the next node to visit for N solutions in parallel at decoding step t_c as follows,

$$c_i^{t_c} = G \cdot \tanh \left(\frac{(h_i^g W_Q)^T (h W_K)}{\sqrt{d_k}} \right), \quad (15)$$

$$p_i^{t_c} = \text{Softmax}(c_i^{t_c}), \quad i \in \{1, 2, \dots, N\}, \quad (16)$$

where $W_Q^g, W_K^g, W_V^g, W_Q, W_K$ are learnable parameter matrices, and G is often set to 10 to control the entropy of $c_i^{t_c}$.

Pertaining to the decoding strategy, we could select the node with the maximum probability in a *greedy* manner or sample a node according to the probability in a *sampling* manner at each decoding step.